Analysis of a PPLN-based cSFG/DFG wavelength conversion for capacities beyond 100 Gb/s

Elaheh Bazouband[1] · Amin Babazadeh[1] · Rahman Nouroozi[1]

Abstract

Wavelength division multiplexing-based networks suffer from blocking probability due to wavelength contention resolution. Such a problem can even be worth when the advanced coherently modulation formats such as M-array quadrature amplitude modulation is used to increase the channel capacity beyond 100 Gbit/s. This paper presents theoretical study of cascaded sum frequency generation and difference frequency generation based tunable wavelength conversion in a periodically poled lithium niobate waveguide as a trivial solution to the wavelength blocking problem when advanced signal modulation formats are considered. It is shown numerically that wavelength conversion of single channel up to 1 Tbit/s would be possible with a 3 cm long wavelength converter.

1 Introduction

Wavelength-Division Multiplexing (WDM) is a promising technique to utilize enormous bandwidth of an optical fiber to be used in telecommunication networks (Yoo 1996). In a WDM-based fiber optical communication network, each data channel is modulated onto an optical carrier with a unique central wavelength. The optical carriers are then multiplexed and transmitted over a fiber line (Yates et al. 1999). In such a network, the blocking probability rises due to a possible wavelength contention when two channels at a same wavelength have to be routed into the same output. One solution to this problem is to convert the wavelength of one signal channel within the transmission bandwidth to the wavelength which has not been occupied in the receiver side (Nouroozi 2010b). Among

✉ Rahman Nouroozi
  rahman.nouroozi@iasbs.ac.ir

  Elaheh Bazouband
  elahe.bazouband.68@gmail.com

  Amin Babazadeh
  babazade@gmail.com

[1] Department of Physics, Institute for Advanced Studies in Basic Sciences, Zanjan 66731-45137, Iran

various wavelength conversion techniques, cascaded sum frequency generation and difference frequency generation (cSFG/DFG) in a periodically poled lithium niobate waveguide has attracted much interest due to a number of helpful features such as; high conversion efficiency, broad wavelength conversion bandwidth within the telecom-band, bit rate and modulation format transparency and no excess noise accumulation during the wavelength conversion (Liu 2012). In addition, the various tunable wavelength conversion functionalities including fixed-in/tunable-out, tunable-in/fixed-out or tunable-in/tunable-out are possible via proper choice of pump-control waves in the cSFG/DFG-based wavelength conversion. The schematic representation of the cSFG/DFG process is illustrated in Fig. 1. Although, using the WDM technique push to increase the capacity of fiber optical network drastically, but the perpetual demand for increasing both bandwidth and capacity of optical network leads to the advent of new hierarchies beyond those are mainly consist of 10 and 40 Gbit/s wavelength channels of a WDM network. Developments in transport technologies such as realization of multi-level modulation format increase the carrying data on one channel to 100 Gbit/s and beyond. In multi-level modulation format by coding several bits in one symbol, symbol rate reduces and narrower channel spacing in WDM network become possible by reduction of optical consumption bandwidth of each channel (Lach and Idler 2011). So, it would be useful to study the capability of the wavelength conversion when such modulation formats are considered. Among different modulation techniques, M-QAM signals with M as symbol number is attractive and has been used for future optical transmission systems. With increasing the M-number, required optical signal to noise ratio (OSNR) is increased to avoid the data loss and bit error rate (BER). Therefore, any system loss such as wavelength conversion induced penalty (including reduced converted signal power due to conversion efficiency) is an important issue in transforming the M-QAM signals. Wavelength conversion based Four Wave Mixing (FWM) and cSFG/DFG for 16/32/64/128-QAM and PAM-4 (4-level pulse amplitude modulation) modulated signals has been demonstrated experimentally in the silicon, compact sige, PPLN, semiconductor optical amplifier and dispersion-engineered silicon nanowire waveguide and highly nonlinear fiber with negligible BER (Wang and Willner 2015; Hu et al. 2016; Giacalone et al. 2015; Hu et al. 2015; Filion et al. 2013; Adams et al. 2014; Long et al. 2016).

In this paper, we theoretically investigate the wavelength conversion based cSFG/DFG in a PPLN waveguide for more different multilevel modulated signals (PM QPSK, PM 8-QAM, PM 16-QAM, PM 32-QAM and PM 64-QAM) which can carry information from 100 Gbit/s up to 1 Tbit/s in each channel. The advantage of this work is being able to optimize and do for every multilevel modulation formats used in optics communication system
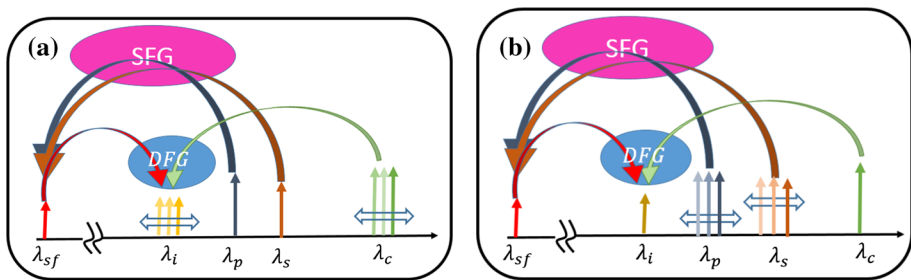

Fig. 1 Schematic representation of cSFG/DFG-based wavelength conversion for fixed-in/tunable-out **a** tunable-in/fixed-out, **b** configurations

and WDM networks and so, it is more general than the works have already done for some specifics modulation formats. Since all parameters are capable of being optimized, this wavelength converter have a wide range of applications in transmitting any kind of modulated signals especially those are used in the next generation of communication systems. The transmission and wavelength conversion of a data for each modulation formats which summarized before are simulated and the optimized full width of half maximum (FWHM) of input signal and the proper waveguide length are calculated. These optimization makes the wavelength conversion process with considerable efficiency and avoidable BER which is a positive point in feasibility and designing high capacity transmission networks in commercial communication systems.

This paper is organized as follows: At first the principle of a cSFG/DFG-based wavelength conversion is introduced and the pulse evaluation during the wavelength conversion along the waveguide is investigated. Then, the full width of half maximum (FWHM) of pulses is achieved to have exact symbol rates in Table 2. Results are discussed about the amount of reached OSNR after wavelength conversion. The proper wavelength converter length for each modulation format to have considerable OSNR (in comparison with ref. Lach and Idler 2011) and negligible BER is calculated.

2 cSFG/DFG-based wavelength conversion

In a χ^2 nonlinear medium, wavelength conversion can be implemented via DFG process (Wang and Xu 2007). A signal wave at wavelength λ_s in C-band interacts with a pump wave at shorter wavelength λ_p to generate a new wavelength converted wave at wavelength λ_i ($1/\lambda_i = 1/\lambda_p - 1/\lambda_s$) which is called idler wave. Due to the energy conservation law, the pump wavelength should be in the 780 nm (near infrared) region to create idler wave in the similar C-band as signal. This is problematic to excite the pump mode selectively in a waveguide which is mono-mode for signal in the C-band and therefore multimode for the pump in near infrared region. The cSFG/DFG process eliminates this problem, where two input waves, i.e. the pump and the signal are in the same 1.5 µm waveband. In this case, two input waves (wavelength λ_s and λ_p) first generate a Sum Frequency (SF) wave at wavelength λ_{sf} ($1/\lambda_{sf} = 1/\lambda_p + 1/\lambda_s$) by the SFG process, then in the successive DFG process, the SF wave interact with the control wave which is again in the C-band (at wavelength λ_c) and generates the desired idler wave at λ_i ($1/\lambda_i = 1/\lambda_p + 1/\lambda_s - 1/\lambda_c$). Therefore, a fundamental mode of SF wave (as the pump wave in DFG process) can be generated selectively by satisfying the quasi phase-matching (QPM) condition via SFG process (Nouroozi 2010b).

In a wavelength conversion scheme via cSFG/DFG process for a fixed signal wavelength, tunable idler wavelength can be obtained by tuning the control wavelength. It can also be applied to give fixed idler wavelength (even if signal is changed) via tuned pump wavelength Fig. 2). Thus by proper adjustment of pump and control waves, fixed-in/tunable-out, tunable-in/fixed-out or tunable-in/tunable-out functions can be performed using cSFG/DFG-based wavelength conversion (Nouroozi 2010b). Figure 1 illustrates the operation principle of the cSFG/DFG-based tunable wavelength conversion schematically. Since the efficient wavelength conversion in the quasi-phase matched-based PPLN waveguide has to be fulfilled with TM polarization of all interacting waves, it is assumed that the input signal and pump waves are TM polarized. To overcome the constraint that cSFG/DFG is inherently polarization-dependent, a polarization diversity scheme in which the two

polarization components of the input telecom signal are converted independently is needed. To provide identical quasi-phase-matching (QPM) and differential group delay (DGD) for the two components it is ideal to utilize the same waveguide twice. This has been accomplished using a polarization maintaining ring configuration with contra-directional single-pass conversion of the two polarization components in the same waveguide. In this way DGD equalization between the two converted polarization components is automatically provided. Indeed, a 4-port circulator and a tunable fiber optic Bragg grating (FBG) for multiplexing of two pumps and signal waves can be used. A fiber optic polarization beam splitter (PBS) with PM-pigtails can then split pumps and signal waves into their TM and TE components. The TM components are launched from one facet into the converter, whereas the TE components are rotated by 90°, following the rotation of the fiber, and launched as TM waves from the opposite facet. For more information please see (Nouroozi 2010b).

The coupled differential equations (Eqs.(2)–(6)) describing the interacting waves and their evolution during cSFG/DFG inside a PPLN waveguide is listed below (Liu 2012). The optical field of the interacting waves is defined to be as follows:

$$E(x, y, z, t) = \frac{1}{2} \Sigma_m A_m(z, t) F_m(x, y) exp(i(\omega_m t - \beta_m z)) + c.c. \tag{1}$$

$A_m(x, y)$ represents the slowly varying complex amplitude of the electric field m ($m = p, c, sf, s, i$) with its transverse field distribution as $F_m(x, y)$. ($\omega_m t - \beta_m z$) is the phase of the corresponding interacting waves with β_m as the propagation constant and ω_m as the corresponding frequency. The coupled mode equations (Eqs.(2)–(6)) which are obtained using the slowly varying envelope approximations, are valid for the pulsed input waves if their bandwidth $\delta\omega$ is significantly smaller than the carrier frequency ω_0, i.e. $\delta\omega/\omega_0 \ll 1$. For the simulations carried out in this paper $\delta\omega/\omega_0 < 0.01$ even for ultra-short pulses of about 100 fs.

$$
\begin{aligned}
&\partial_z a_s(z, t) + \beta_s' \partial_t a_s(z, t) + i\frac{\beta_s''}{2} \partial_t^2 a_s(z, t) - \frac{\alpha_s}{2} a_s(z, t) \\
&= -i\kappa_{(s,SFG)} \nu_{(SFG)} a_p^*(z, t) a_{sf}(z, t) \exp(i\Delta\beta_{SFG} z),
\end{aligned}
\tag{2}
$$

$$
\begin{aligned}
&\partial_z a_p(z, t) + \beta_p' \partial_t a_p(z, t) + i\frac{\beta_p''}{2} \partial_t^2 a_p(z, t) - \frac{\alpha_p}{2} a_p(z, t) \\
&= -i\kappa_{(p,SFG)} \nu_{(SFG)} a_s^*(z, t) a_{sf}(z, t) \exp(i\Delta\beta_{SFG} z),
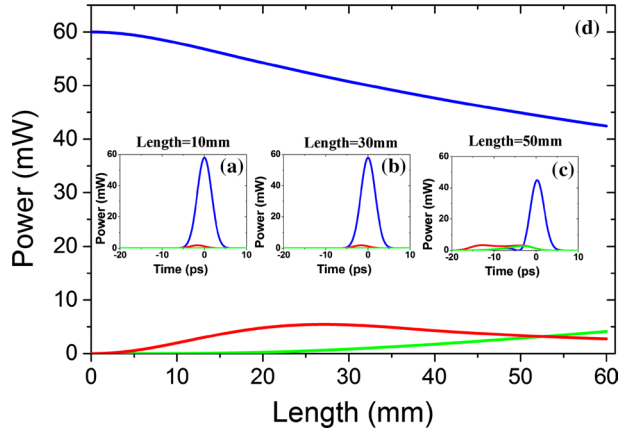\end{aligned}
\tag{3}
$$

$$
\begin{aligned}
&\partial_z a_{sf}(z, t) + \beta_{sf}' \partial_t a_{sf}(z, t) + i\frac{\beta_{sf}''}{2} \partial_t^2 a_{sf}(z, t) - \frac{\alpha_{sf}}{2} a_{sf}(z, t) \\
&= -i\kappa_{(sf,SFG)} \nu_{(SFG)} a_s(z, t) a_p(z, t) \exp(-i\Delta\beta_{SFG} z) \\
&\quad - i\kappa_{(sf,DFG)} \nu_{(DFG)} a_i(z, t) a_c(z, t) \exp(-i\Delta\beta_{DFG} z),
\end{aligned}
\tag{4}
$$

$$
\begin{aligned}
&\partial_z a_c(z, t) + \beta_c' \partial_t a_c(z, t) + i\frac{\beta_c''}{2} \partial_t^2 a_c(z, t) - \frac{\alpha_c}{2} a_c(z, t) \\
&= -i\kappa_{(c,DFG)} \nu_{(c,DFG)} a_{sf}(z, t) a_i^*(z, t) \exp(i\Delta\beta_{DFG} z),
\end{aligned}
\tag{5}
$$

Table 1 Parameters used in simulations with $\kappa_{SFG} \simeq \kappa_{DFG} = 0.55$ 1/m and Λ_{QPM}=16.6 μm

Wavelength (nm)	$\lambda_p = 1540$	$\lambda_s = 1550$	$\lambda_{sf} = 772.49$	$\lambda_c = 1535$	$\lambda_i = 1555.1$
α (dB/cm)	0.15	0.15	0.3	0.15	0.15
n_{eff}	2.1455	2.1452	2.1877	2.1456	2.1450
$\beta' \times 10^{-9}$ (s/m)	7.3032	7.3023	7.6225	7.3036	7.3019
$\beta'' \times 10^{-25}$ (s^2/m)	1.0934	1.0669	4.0660	1.1066	1.0535

Fig. 2 The power evaluation of signal (blue), SF (red) and idler (green) pulses during the 60 mm long PPLN waveguide. Insets: Temporal evolution of the signal, SF and idler pulses after propagation as 10 mm (a), 30 mm (b) and 50 mm (c) inside the PPLN waveguide. (Color figure online)

$$\partial_z a_i(z,t) + \beta_i' \partial_t a_i(z,t) + i\frac{\beta''}{2}\partial_t^2 a_i(z,t) - \frac{\alpha_i}{2}a_i(z,t)$$
$$= -i\kappa_{(i,DFG)}v_{(i,DFG)}a_{sf}(z,t)a_c^*(z,t)\exp(i\Delta\beta_{DFG}z). \qquad (6)$$

$\Delta\beta_{SFG} = \beta(\omega_{sf}) - \beta(\omega_s) - \beta(\omega_p) - \frac{2\pi}{\Lambda_{QPM}}$, and $\Delta\beta_{DFG} = \beta(\omega_{sf}) - \beta(\omega_i) - \beta(\omega_c) - \frac{2\pi}{\Lambda_{QPM}}$, represent the phase mismatch in the SFG and DFG interactions respectively. $\kappa_{(x,SFG)}$ and $\kappa_{(x,DFG)}$ are the coupling coefficients and $v_{(SFG)}$ and $v_{(DFG)}$ are the overlapping integrals of the interacting waves for the SFG and DFG interactions respectively and x=p, c, sf, s and i. β_x' is the inverse of the group velocity, β_x'' is the group velocity dispersion (GVD) parameter and α_i is the attenuation coefficient for i= p, c, sf, s and i.

The split-step Fourier method (Agrawal 2001) together with the runge-kutta algorithm is used to solve the coupled mode equations (Eqs.(2)–(6)) numerically with the waveguide parameters listed in the Table 1 (Nouroozi 2010b). The signal wave assumed to be a Gaussian pulse with 60 mW input peak power (P_s) (Babazadeh et al. 2016):

$$A_s(z,t) = \sqrt{P_s}exp(-2\ln(2)\frac{t^2}{\tau^2}), \qquad (7)$$

with τ as the initial FWHM and $A_s(z,t)$ as the signal mode amplitude. Results of the power evolution along a 60 mm PPLN channel waveguide when a 4 ps input signal pulse is considered are illustrated in Fig. 2. As it is shown during the first half of the propagation length, the SF pulse is being generated via SFG process between signal pulse and a continuous wave pump. Then the power of SF pulse decreases in the rest of the waveguide by

transferring its energy to generated idler pulse via DFG process with a continuous control wave.

The pulses with different wavelengths propagate with different group velocities in a PPLN waveguide. This leads to a group velocity dispersion (GVD) and group velocity mismatch (GVM) between pulses in the cSFG/DFG process. Therefore, a temporal walk-off (represented in Eq. (8)) between the SF pulse in the IR range and the signal/idler pulses in the c-band results which itself causes decreasing in the temporal overlapping of the interaction between SF pulse with the signal/idler pulses. This is shown in the insets of the Fig. 2 where the SFG and DFG interactions are accumulated in region where the tailing edge of the signal/idler pulses and the leading edge of SF pulse are met. The $L_{walk-off}$ is the length that the walk-off between signal pulse and the SF pulse is calculated and is given by:

$$L_{walk-off} = \frac{\Delta\tau}{v_{sf}^{g\,-1} - v_{s}^{g\,-1}},$$

(8)

where $\Delta\tau$ is FWHM of signal pulse and v_{s}^{g} and v_{sf}^{g} are group velocity of signal and SF pulses respectively. Moreover, the power evolution of signal and idler pulses during their nonlinear interaction versus time is illustrated in Fig. 3. Due to GVD and temporal walk-off during the 60 mm of interaction length (in this spacial example), the generated idler pulse is broadened and lagged behind the signal pulse. In addition, a small pulse is generated behind the signal because of the back conversion process between the generated idler and remaining pump to reproduce the signal pulse. Consequently, the wavelength conversion process causes temporal broadening and distortion of transmitted pulses. Such a pulse broadening/distortion reduces the optical OSNR in an optical telecommunication channel. Here in this paper reduction of the OSNR caused by cSFG/DFG-based wavelength conversion assumed as a noise source and is studied for different modulation formats which are used for capacities beyond 100 Gbit/s WDM networks.

Fig. 3 The power evolution of signal (blue) and idler (green) pulses during their nonlinear interaction versus time in a 60 mm long waveguide. The GVD and temporal walk-off case the idler broadening. An additional signal pulse generation is due to back conversion process between the generated idler and remaining pump. (Color figure online)
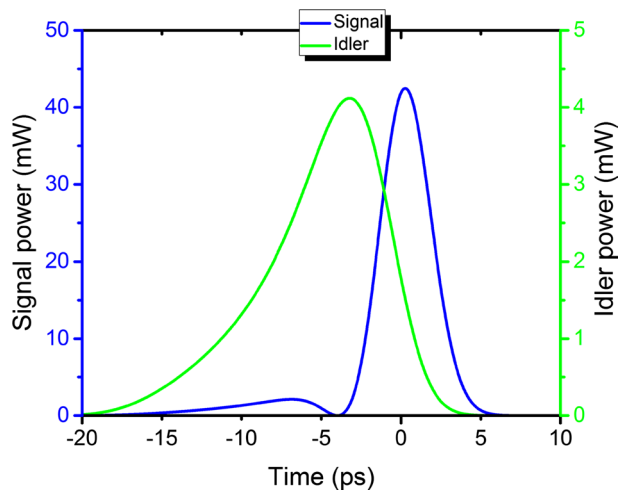
3 Signal modulation and its wavelength conversion

Transmission capacities together with their modulation format and related symbol rates used for cSFG/DFG-based wavelength conversion of single channels are summarized in Table 2. The last row in the Table 2 shows the minimum required OSNR for optical data transformation in each bitrate and related modulation format. Data are extracted from (Lach and Idler 2011).

Wavelength conversion of signals with 100, 200, 400 and 1000 Gbit/s bitrates are analyzed. Such signals built up with short pulses. As an example, for a signal with 1000 Gbit/s bitrate and the return to zero format, the pulses are as short as 500 fs. Therefore, dispersion together with nonlinear interactions can affect their temporal shape. Change in the pulse shapes induces an inter symbol interference (ISI) between pulses and therefore reduces the OSNR of the channel. If the value of OSNR drops below the listed OSNR values in the Table 2 (here due to induced power penalty via wavelength conversion), then the channel cannot be resolved and its data are lost. This would end up to a limitation to use that format with desired capacity. In addition, there are the limitations for modulator to modulate and demodulate these high speed bit rates. The multilevel modulation formats by using M bits in each symbols resolve these problems as the time duration of pulse increases and the speed of modulating reduces. Furthermore, multi-level coding reduces optical bandwidth consumption of channel and enables WDM transmission with narrower dense WDM channel spacing.

3.1 Wavelength conversion of 100 and 200 Gbit/s

According to the OSNR listed in Table 2, the PM QPSK modulation has lowest nedded OSNR and therefore appears as the best performing 100 Gbit/s modulation format and is widely been used (Fludger et al. 2007; Chandrasekhar et al. 2008; Gavioli et al. 2010). In contrast to direct detection, no precoding transmitters is required because the optical phase is directly recovered by coherent mixing the received optical signal with a narrow linewidth laser as local oscillator. For modulation format beyond 100 Gbit/s the major focus is on multilevel modulation format based on QAM together with coherent detection. Recently, PM M-QAM scheme is utilized to achieve a channel rate of 200 Gbit/s, e.g. the PM 16-QAM has been realized by multilevel generation using passive combination of binary signals (Gnauck et al. 2010; Winzer et al. 2010).

The high bit rate of these two capacities is reduced to 32 Gbaud symbol per second by using the mentioned modulation techniques where in PM QPSK modulation, 4 bits are transmitted in each symbol where 2 bits are carried by QPSK modulation format. Then they are multiplied by 2 for polarization multiplexed. For the PM 16-QAM (4 for 16-QAM

Table 2 The characteristics of the 100, 200, 400 and 1000 Gbit/s transmission capacities in different modulation formats

Modulation format	PM QPSK	PM 16-QAM	PM 64-QAM	PM 8-QAM	PM 64-QAM	PM 32-QAM
Bitrate (Gbit/s)	100	200	400	400	1000	1000
Symbol rate (Gbaud)	32	32	43	85	107	128
OSNR (dB)	9.8	16.8	24.3	17.8	28.3	16

× by 2 for PM), 8 bits are transmitted in each symbol to achieve capacities in the range of 100 Gbit/s and 200 Gbit/s. The FWHM of the input pulse satisfying such a signal in a return to zero (RZ) format is 7.5 ps. The input pulse train for this symbol rate is shown in the inset of the Fig. 4. As it is shown in Fig. 4, the FWHM of output idler pulses of 10.5 ps is achieved which indicates an increase of about forty percentage in comparison with input signal pulses. Since the temporal walk-off length ($L_{walk-off} = 21 mm$) is shorter than the PPLN waveguide ($L = 60$ mm), such a broadening causes negligible ISI between transmitted wavelength converted idler pulses for the capacities of 100 and 200 Gbit/s which are modulated with PM QPSK and PM 16-QAM respectively.

3.2 Wavelength conversion of 400 and 1000 Gbit/s

Since the main technical limitation for implementation of the system with high symbol rates are the digital to analog converter (DAC) and analog to digital converter (ADC), therefore, the 400 Gbit/s single carrier with PM 64-QAM (that carry 12 bits in each symbol, 6 bits for 64-QAM × by 2 for PM) can be a feasible option at a realistic symbol rates of likely 43 Gbaud . For such a single channel the train of RZ pulses with ∼ 5.5 *ps* temporal FWHM is chosen. Figure 5a shows the input and transmitted pulses for this symbol rate. The optimum length for this modulation is calculated to be 49 mm. This length is sufficient to reach OSNR (∼ 25.23) higher than the required amount in Table 2 (Fig. 5a). The inphase-quadrature diagram of this modulation also shows reasonable accommodation of the received data as it is illustrated in Fig. 5b.

For the same bitrate rate of 400 Gbit/s with 85 Gbaud symbol rate and the modulation format of PM 8-QAM (6 bits are carried in each symbol, 3 for 8-QAM × by 2 for PM), the input RZ pulses of ∼ 3 *ps* are considered. Although, the calculated OSNR of 6.77 dB (Fig. 6a) for this modulation is below the required OSNR according to Table 2 and the I-Q diagram shows scattered islands for received signal (Fig. 6b).

Nevertheless, decreasing the noise is possible when the propagation length is optimized for this modulation format. This is calculated to be 25 mm. Figure 7a, b shows the transmitted pulse train and the I-Q diagram of the system after optimization of the PPLN length, respectively.

Fig. 4 The transmitted cSFG/DFG-based wavelength converted idler pulse train for 32 Gbaud. Inset shows the input signal return-to-zero pulse train
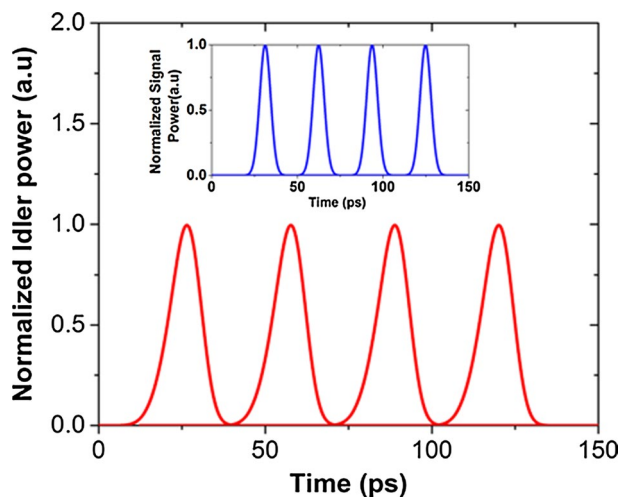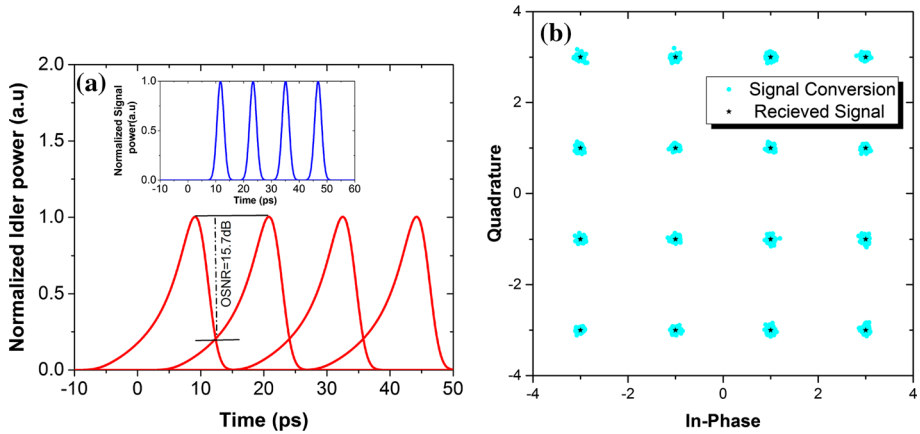
Fig. 5 **a** The output idler pulse train for 43 Gbaud symbol rate. The inset diagram shows the input signal pulse train. The I-Q diagram of the 43 Gbaud symbol rate for PM 64-QAM modulation is shown in **b**
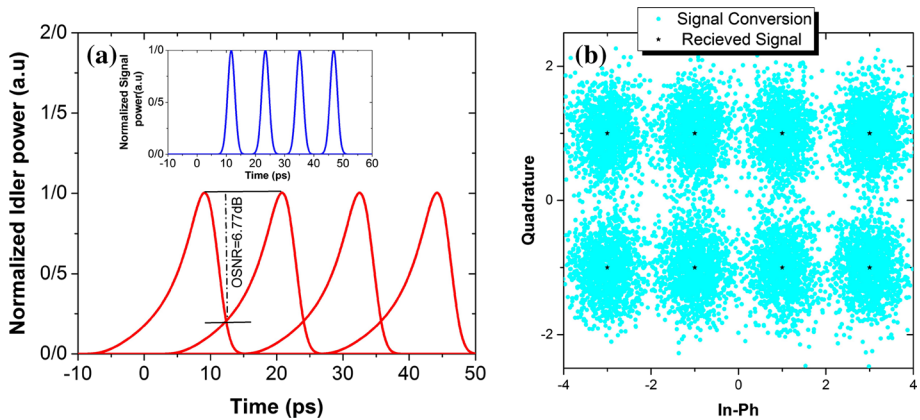

Fig. 6 **a** The output idler pulse train for 85 Gbaud symbol rate after the optimization of the waveguide's length. The inset diagram shows the input signal pulse train. The I-Q diagram of the 85 Gbaud symbol rate for PM 8-QAM modulation is shown in **b**

The two 1 Tbit/s with the modulation formats of PM 32-QAM and PM 64-QAM (which respectively carry 10 and 12 bits in each symbol) in the Table 2 are added only to indicate the need of very challenging high symbol rate. Therefore, only multicarrier solution are suggested for 1 Tbit/s transmission (Lach and Idler 2011), but checking the wavelength conversion of single carrier 1 Tbit/s with high M-QAM modulation can be useful for more advanced telecommunication systems. Now we consider the symbol rates used for capacity of 1 Tbit/s in Table 2. The FWHMs of pulses that are chosen for symbol rates of 107 and 128 Gbaud are 2.33 ps and 1.95 ps respectively. The simulation shows that OSNR for 60 mm length of the PPLN for the symbol rates of 107 and 128 Gbaud are 6.05 dB and 5.27 dB respectively (Fig. 8). The optimum PPLN waveguide length for the wavelength conversion of such high bitrates are calculated to be 17 mm and 21 mm, respectively. Since the efficiency of the wavelength conversion directly
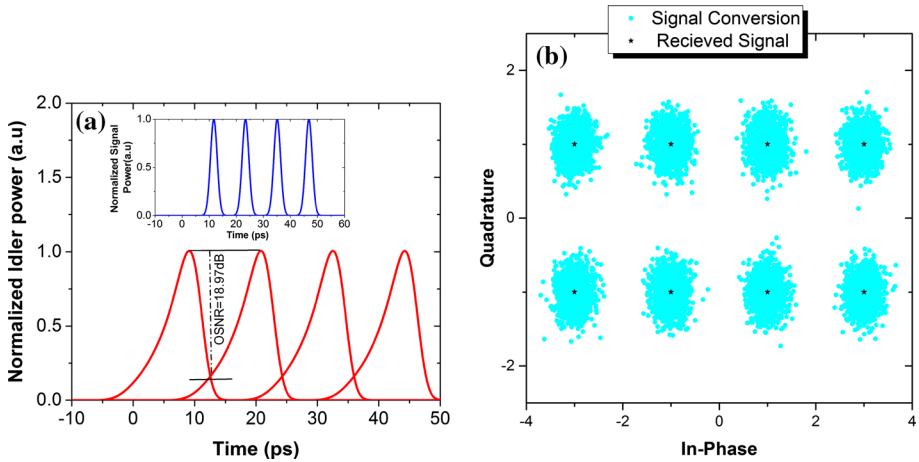
Fig. 7 **a** The output idler pulse train for 85 Gbaud symbol rate after the optimization of the waveguide's length. The inset diagram shows the input signal pulse train. The I-Q diagram of the 85 Gbaud symbol rate for PM 8-QAM modulation is shown in **b**
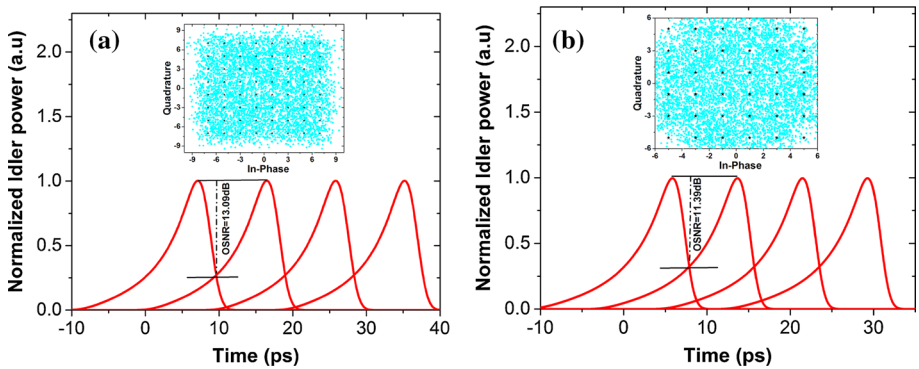

Fig. 8 The output signal train for 107 (left) and 128 (right) Gbaud symbol rate. Insets show the I-Q diagram of the corresponding symbole rate for PM 64-QAM (left) and PM 32-QAM (right) modulation formats

depended on the interaction length, there is a trade-off between high symbol rate and the efficiency.

4 Conclusions

Although generation and detection of high bit rate optical telecommunication signals are suggested for future WDM-based fiber networks, required functionalities in a realistic network are challenging. One of them could be the wavelength contention resolution in the routing nodes of the network. This paper summarized the effect of using cSFG/DFG-based wavelength conversion as powerful solution of the problem in the transmitted wavelength converted signals. This is accompanied with high bit rated advanced coherently modulated

signal of 100, 200, 400 Gbit/s and also for 1 Tbit/s. It is shown that signal with 32 Gbaud symbol/s which is correspond to generate 100 Gbit/s of PM QPSK format and 200 Gbit/s of PM 16-QAM format can be wavelength converted in a 60 mm long PPLN waveguide. This can be achieved in a 25 mm long waveguide when symbol rate is increased to 85 Gbaud/s for 400 Gbit/s channel whereas for 1 Tbit/s channel with above 100 Gbaud/s symbol rate waveguide length should be shorten down to 17 mm.

Since all results and parameters listed above are applicable to reach via waveguide fabrication, the wavelength converters with specific lengths have a wide range of applications in the next generation of communication systems. Results presented in this paper may have found applications in practical implementation of future ultra high capacity WDM-based fiber telecom networks.

References

Adams, R., Spasojevic, M., Chagnon, M., Malekiha, M., Li, J., Plant, D.V., Chen, L.R.: Wavelength conversion of 28 GBaud 16-QAM signals based on four-wave mixing in a silicon nanowire. Opt. Express **22**(4), 4083–4090 (2014). https://doi.org/10.1364/OE.22.004083

Agrawal, G.G.P.: Nonlinear Fiber Optics, 3rd edn. Academic Press, Boston (2001). https://doi.org/10.3367/UFNr.0160.199005k.0151

Babazadeh, A., Nouroozi, R., Sohler, W.: Phase engineered wavelength conversion of ultra-short optical pulses in TI: PPLN waveguides. Opt. Commun. **361**, 143–147 (2016). https://doi.org/10.1016/j.optcom.2015.09.066

Chandrasekhar, S., Liu, X.: OFC/NFOEC 2008 - 2008 Conference on Optical Fiber Communication/National Fiber Optic Engineers Conference (Dli), 8 (2008). https://doi.org/10.1109/OFC.2008.4528546

Filion, B., Ng, W.C., Nguyen, A.T., Rusch, L.A., LaRochelle, S.: Wideband wavelength conversion of 16 Gbaud 16-QAM and 5 Gbaud 64-QAM signals in a semiconductor optical amplifier. Opt. Express **21**(17), 19825–19833 (2013). https://doi.org/10.1364/OE.21.019825

Fludger, C.R., Duthel, T., van den Borne, D., Schulien, C., Schmidt, E.D., Wuth, T., de Man, E., Khoe, G.D., de Waardt, H.: in *Optical Fiber Communication Conference and Exposition and The National Fiber Optic Engineers Conference* (Optical Society of America, 2007), p. PDP22

Gavioli, G., Torrengo, E., Bosco, G., Carena, A., Savory, S.J., Forghieri, F., Poggiolini, P.: Ultra-narrow-spacing 10-channel 1.12 Tb/s D-WDM long-haul transmission over uncompensated SMF and NZDSF. IEEE Photon. Technol. Lett. **22**(19), 1419–1421 (2010). https://doi.org/10.1109/LPT.2010.2062174

Giacalone, M., Meloni, G., Fresi, F., Potì, L.: A numerical and experimental comparison of a wavelength conversion for a 200 Gbit/s super-channel in a periodically poled lithium niobate waveguide. Opt. Quant. Electron. **47**(6), 1465–1470 (2015). https://doi.org/10.1007/s11082-015-0118-1

Gnauck, A.H., Winzer, P.J., Chandrasekhar, S., Liu, X., Zhu, B., Peckham, D.W.: in *Optical Fiber Communication Conference* (Optical Society of America, 2010), p. PDPB8. https://doi.org/10.1364/OFC.2010.PDPB8

Hu, H., Jopson, R., Gnauck, A., Dinu, M., Chandrasekhar, S., Xie, C., Randel, S.: Parametric amplification, wavelength conversion, and phase conjugation of a 2.048-Tbit/s WDM PDM 16-QAM signal. J. Lightwave Technol. **33**(7), 1286–1291 (2015)

Hu, X., Zeng, M., Long, Y., Liu, J., Zhu, Y., Zou, K., Zhang, F., Fu, L., Wang, J.: Phase conjugated and transparent wavelength conversions of Nyquist 16-QAM signals employing a single-layer graphene coated fiber device. Sci. Rep. **6**, 1–8 (2016)

iu, S.: All-optical signal processing using cascaded quadratic interaction in periodically poled lithium niobate waveguide. Ph.D. thesis (2012)

Lach, E., Idler, W.: Modulation formats for 100G and beyond. Opt. Fiber Technol. **17**(5), 377 (2011). https://doi.org/10.1016/j.yofte.2011.07.012

Long, Y., Wang, A., Zhou, L., Wang, J.: All-optical wavelength conversion and signal regeneration of PAM-4 signal using a silicon waveguide. Opt. Express **24**(7), 7158–9167 (2016). https://doi.org/10.1364/OE.24.007158

Nouroozi, R.: All optical wavelength conversion and parametric amplification in Ti : PPLN channel waveguides for telecommunication applications. Ph.D. thesis (2010)

Wang, J., Willner, A.E.: in *Applications of Digital Signal Processing through Practical Approach* (IntechO-
    pen, 2015)
Wang, Y., Xu, C.Q.: Analysis of picosecond-pulse wavelength conversion based on cascaded sum-frequency
    generation and difference-frequency generation in quasi-phase-matched LiNbO 3 waveguides. Opt.
    Eng. **46**(5), 055003 (2007). https://doi.org/10.1117/1.2740751
Winzer, P.J., Gnauck, A.H., Doerr, C.R., Magarini, M., Buhl, L.L.: Spectrally efficient long-haul optical
    networking using 112-Gb/s polarization-multiplexed 16-QAM. J. Lightwave Technol. **28**(4), 547–556
    (2010)
Yates, J.M., Rumsewicz, M.P., Lacey, J.P.R.: Wavelength converters in dynamically-reconfigurable WDM
    networks. IEEE Commun. Surv. Tutor. **2**(2), 2 (1999). https://doi.org/10.1109/COMST.1999.5340515
Yoo, S.J.B.: Wavelength conversion technologies for WDM network applications. J. Lightwave Technol.
    14(6), 955–966 (1996). https://doi.org/10.1109/50.511595